Supplementary Information:

Composition-structure-property relationships of polyethylene vitrimers crosslinked by 8-arm POSS

Mikaela Sadri[1], Andrew Barbour[1], Travis L. Thornell[2], J. Kent Newman[2], Zhe Qiang[1]*

[1]School of Polymer Science and Engineering, The University of Southern Mississippi, Hattiesburg, MS, 39406

[2]U. S. Army Engineer Research and Development Center, Geotechnical and Structures Laboratory, Vicksburg, MS 39180

Correspondence to: Z. Q. (Email: zhe.qiang@usm.edu)

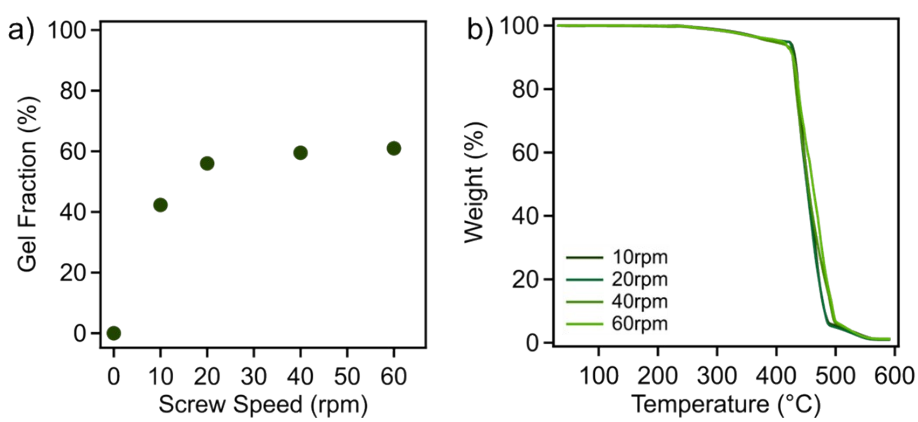

Figure S1. Impact of shear speed on the (a) gel fraction and (b) thermal degradation in N_2 of PE_v-1.0, where samples are recirculated for 5 min.

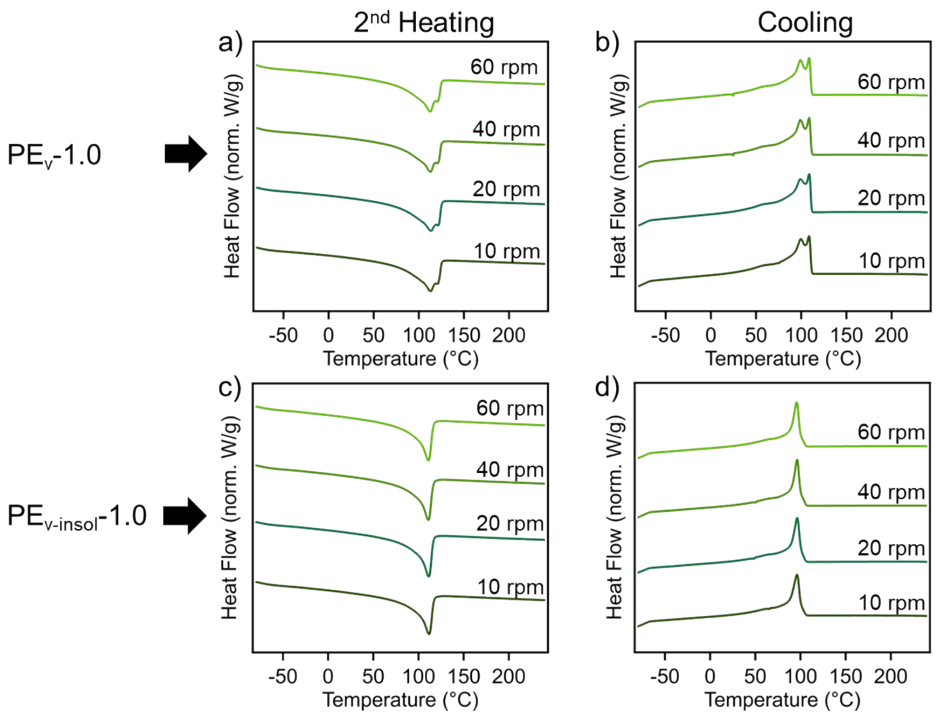

Figure S2. Impact of screw speed on the DSC 2nd heating and cooling thermograms of PE_v-1.0 ((a) and (b)) and $PE_{v\text{-}insol}$-1.0 ((c) and (d)).

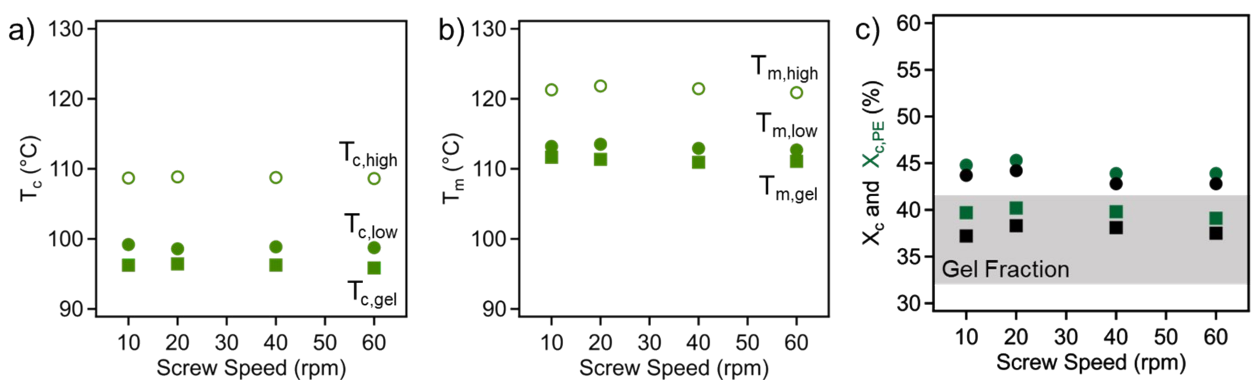

Figure S3. (a) Crystallization temperature (T_c), melting temperature (T_m), and (c) degree of crystallization (X_c) as a function of screw speed for PE_v-1.0 samples.

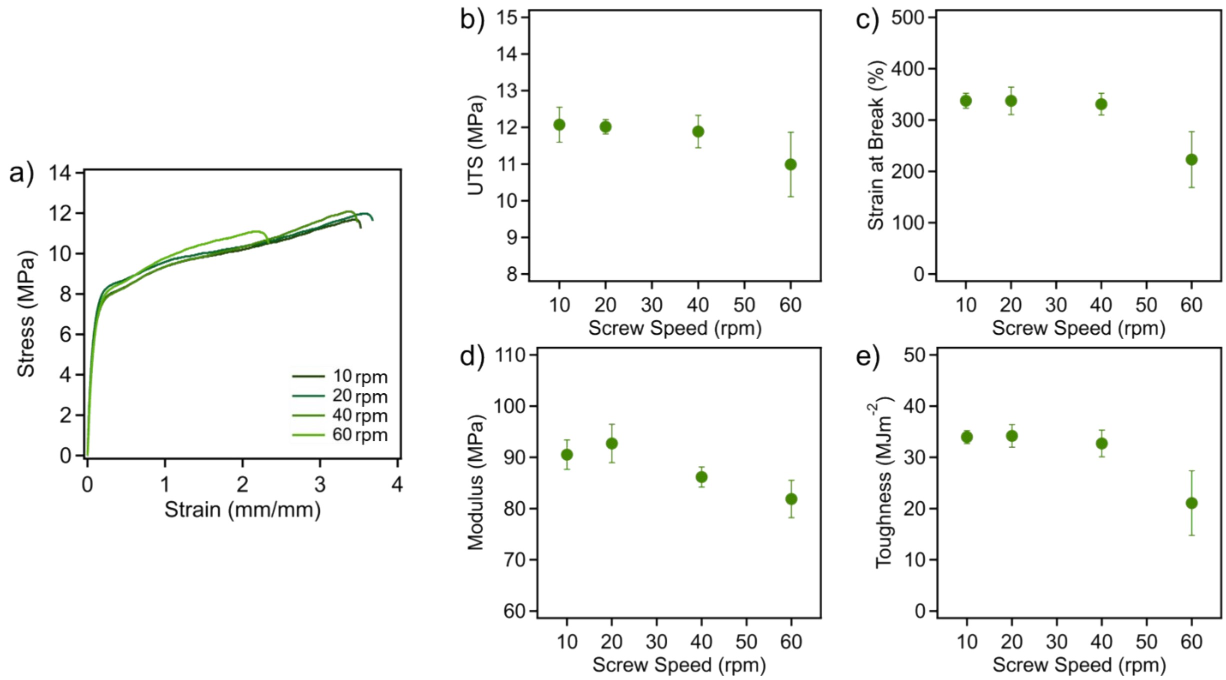

Figure S4. Mechanical properties as a function of screw speed, demonstrating the influence of shear speed on the (a) stress-strain curves, (b) UTS, (c) strain at break, (d) modulus, and (e) fracture toughness.

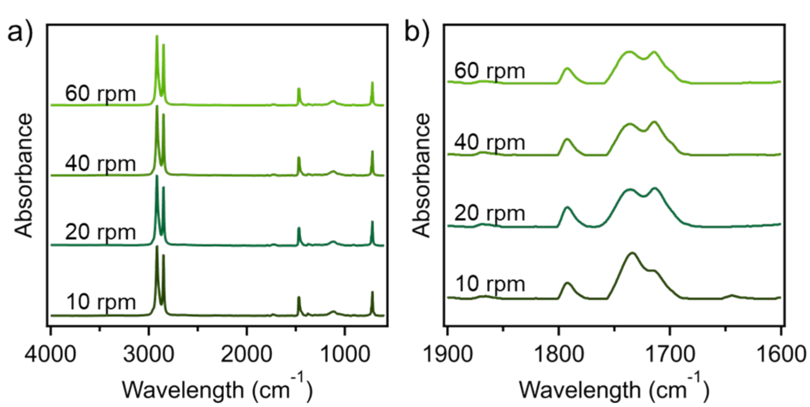

Figure S5. (a) FTIR spectra of PE_v-1.0 compounded at different screw speeds, and (b) expanded view of the bands corresponding to the epoxy-anhydride reactions.

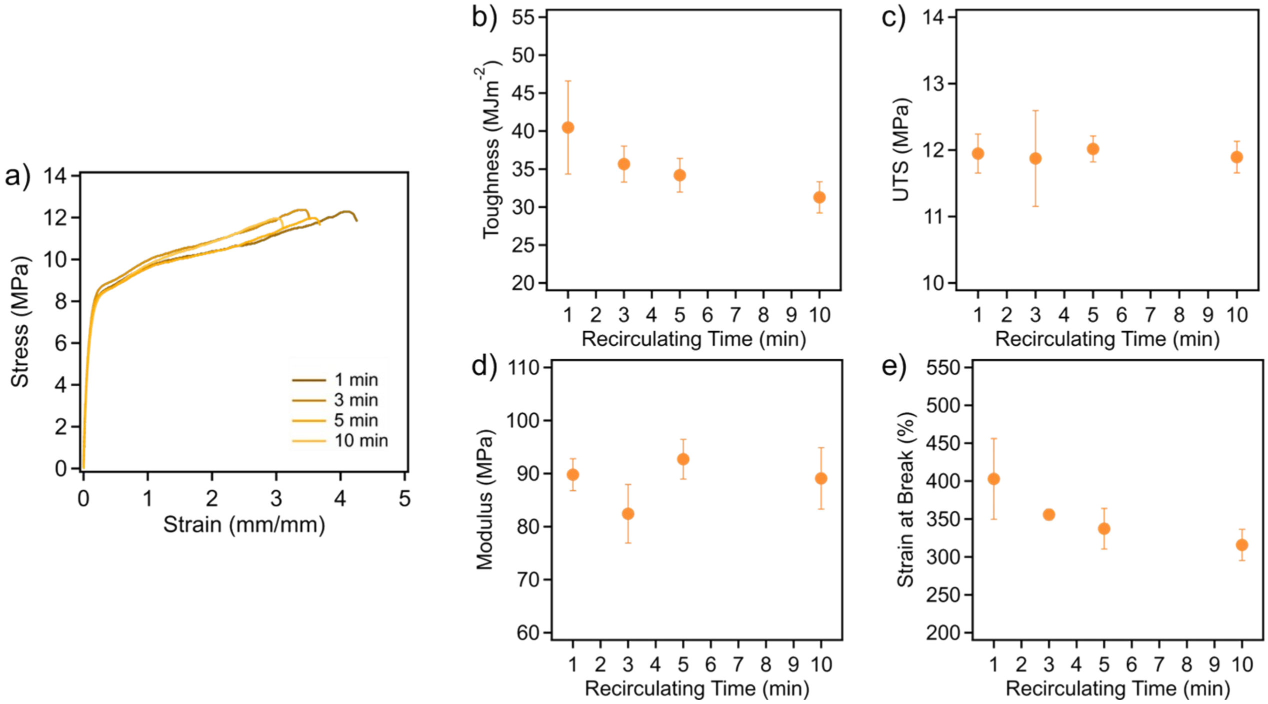

Figure S6. Mechanical properties as a function of recirculation time, demonstrating the influence of shear time on the (a) stress-strain curves, (b) fracture toughness, (c) UTS, (d) modulus, and (e) strain at break.

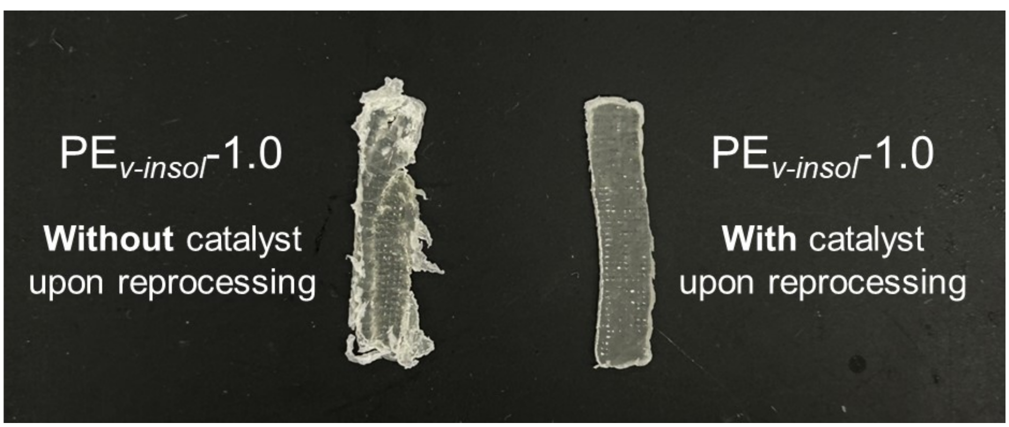

Figure S7. Results of melt processing $PE_{v\text{-}insol}$-1.0 samples when they were reprocessed without the reintroduction of catalyst (left) and with the reintroduction of 1 wt.% catalyst upon reprocessing (right).

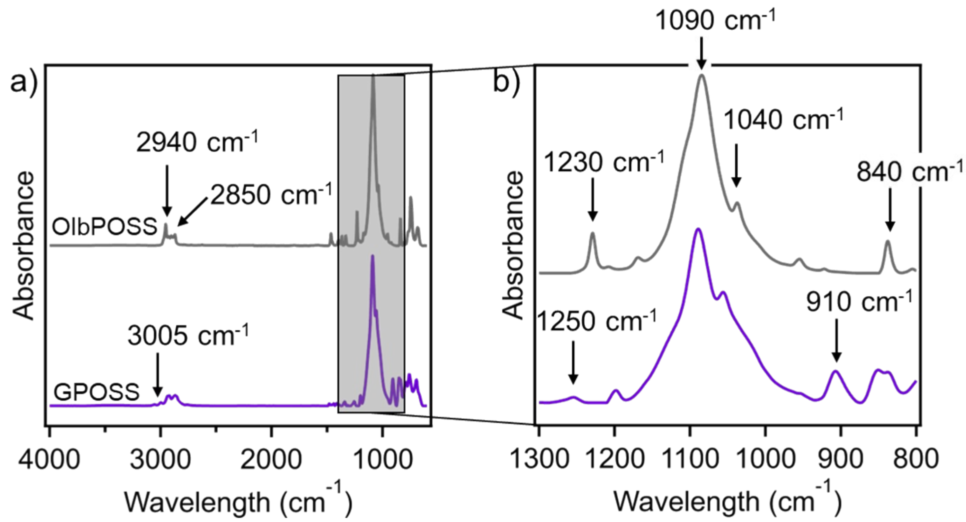

Figure S8. FTIR of neat GPOSS (purple) and OIbPOSS (gray), where (a) shows the full spectrum, and (b) shows a closeup range of the fingerprint region. The bands within (a) can be attributed to alkane stretching (2940 and 2850 cm^{-1}) found within the branches of both crosslinkers, as well as the C-H stretching from the epoxide group (3005 cm^{-1}) within GPOSS. Additionally, within (b), the bands at 1090 and 1040 cm^{-1} for both POSS structures can be attributed to Si-O stretching due to the Si-O-Si bonds found within the POSS cages. The band at 840 cm^{-1} also correlates to the stretching of Si-C bonds. Looking specifically at OIbPOSS, the band at 1230 cm^{-1} corresponds to the CH_3, a function of skeletal vibration from the $C(CH_3)_3$ groups. Within the GPOSS, the 1250 and 910 cm^{-1} bands correspond to asymmetric ring stretching and symmetric ring stretching, respectively, from the epoxide group.

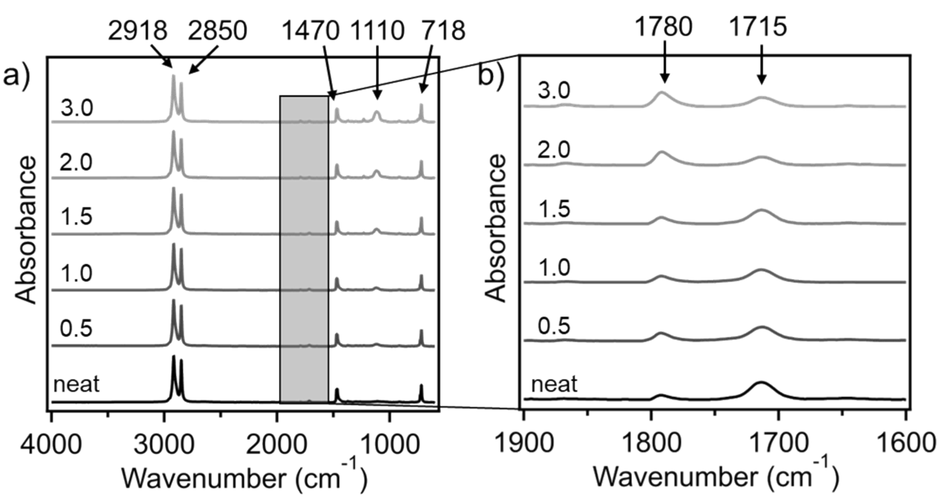

Figure S9. (a) FT-IR spectra of PE_{neat} and PE_b with varying molar ratios of PFGs to MA using OIbPOSS, where (b) shows a closeup range of the bands corresponding to the region where epoxy-anhydride reactions could be seen within PE_v samples.

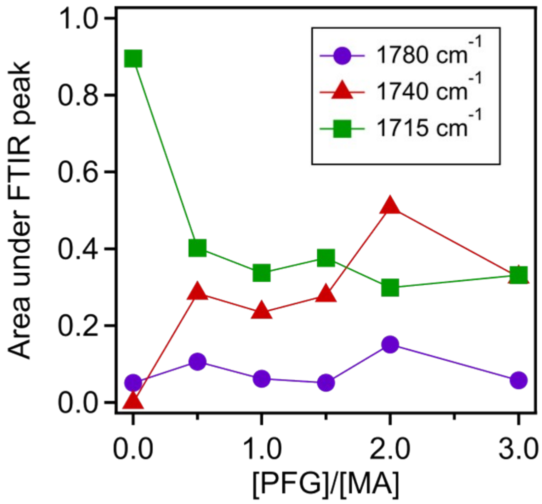

Figure S10. Integrated peak area as a function of GPOSS content for the peaks corresponding to the epoxy-anhydride curing.

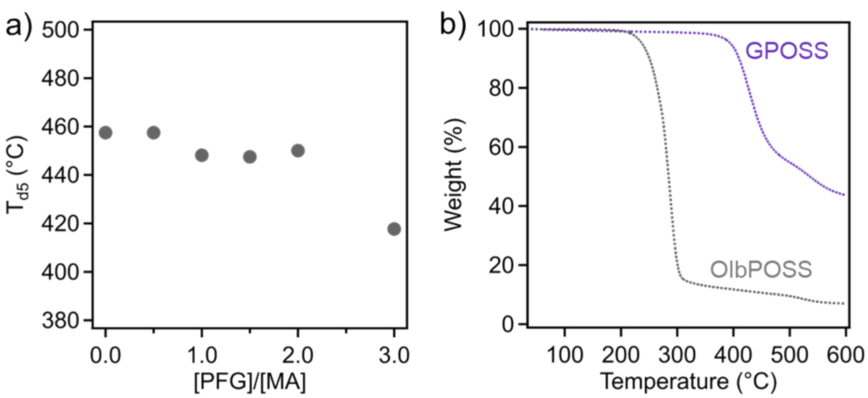

Figure S11. a) T_{d5} of PE_b samples and b) TGA curves of neat OIbPOSS and GPOSS in N_2.

Table S1. Key temperatures and characteristics of the vitrimer components samples as a function of POSS loading, PE_v, $PE_{v\text{-}sol}$, and $PE_{v\text{-}insol}$, including degree of crystallization and distinctive lamellar thicknesses.

Name	**T_m Low (°C)**	**T_m High (°C)**	**T_c Low (°C)**	**T_c High (°C)**	**ΔH_m (J/g)**	***χ_c (%)***	***$\chi_{c,PE}$ (%)***	***L Low (nm)***	***L High (nm)***
PE_{neat}	-	121.9	-	106.6	142.6	48.7	48.7	-	8.8
PE_v-0.5	**114.5**	122.4	99.1	**108.8**	138.3	47.2	47.8	6.4	9.0
PE_v-1.0	**113.5**	121.8	98.6	**108.9**	129.5	44.2	45.3	6.2	8.8
PE_v-1.5	**113.3**	121.8	**97.6**	108.4	132.4	45.2	46.9	6.2	8.8
PE_v-2.0	**113.1**	121.5	98.8	109.0	141.0	48.1	50.6	6.1	8.6
PE_v-3.0	**112.5**	121.8	97.7	109.0	131.3	44.8	48.2	6.0	8.7
$PE_{v\text{-}sol}$-0.5	-	116.8	-	104.4	131.7	44.9	44.9	-	7.0
$PE_{v\text{-}sol}$-1.0	-	117.7	-	106.3	140.1	47.8	47.8	-	7.3
$PE_{v\text{-}sol}$-1.5	-	114.3	-	102.9	134.5	45.9	45.9	-	6.4
$PE_{v\text{-}sol}$-2.0	-	118.5	-	104.9	140.4	47.9	47.9	-	7.5
$PE_{v\text{-}sol}$-3.0	-	120.8	-	109.8	142.5	48.6	48.6	-	8.3
$PE_{v\text{-}insol}$-0.5	111.8	-	96.4	-	107.5	36.7	37.6	5.8	-
$PE_{v\text{-}insol}$-1.0	111.1	-	96.6	-	113.7	38.8	40.7	5.7	-
$PE_{v\text{-}insol}$-1.5	111.0	-	96.0	-	111.0	37.9	40.4	5.7	-
$PE_{v\text{-}insol}$-2.0	111.5	-	95.9	-	109.2	37.3	41.2	5.8	-
$PE_{v\text{-}insol}$-3.0	110.2	-	96.1	-	110.7	37.8	42.7	5.6	-
PE_b-0.5	-	121.7	-	106.6	140.8	48.1	48.4	-	8.7
PE_b-1.0	-	120.5	-	106.6	141.4	48.3	49.1	-	8.2
PE_b-1.5	-	121.9	-	106.8	139.8	47.7	48.9	-	8.8
PE_b-2.0	-	120.7	-	106.4	140.9	48.1	49.7	-	8.3
PE_b-3.0	-	121.9	-	105.8	129.6	44.2	46.5	-	8.8
PE_v-1.0-DGEBA	111.9	122.2	94.2	108.9	128.4	41.8	42.8	5.9	8.9
$PE_{v\text{-}sol}$-1.0-DGEBA	-	123.1	-	108.3	139.1	47.5	48.7	-	9.4
$PE_{v\text{-}insol}$-1.0-DGEBA	109.6	-	93.8	-	113.4	38.5	39.7	5.4	-

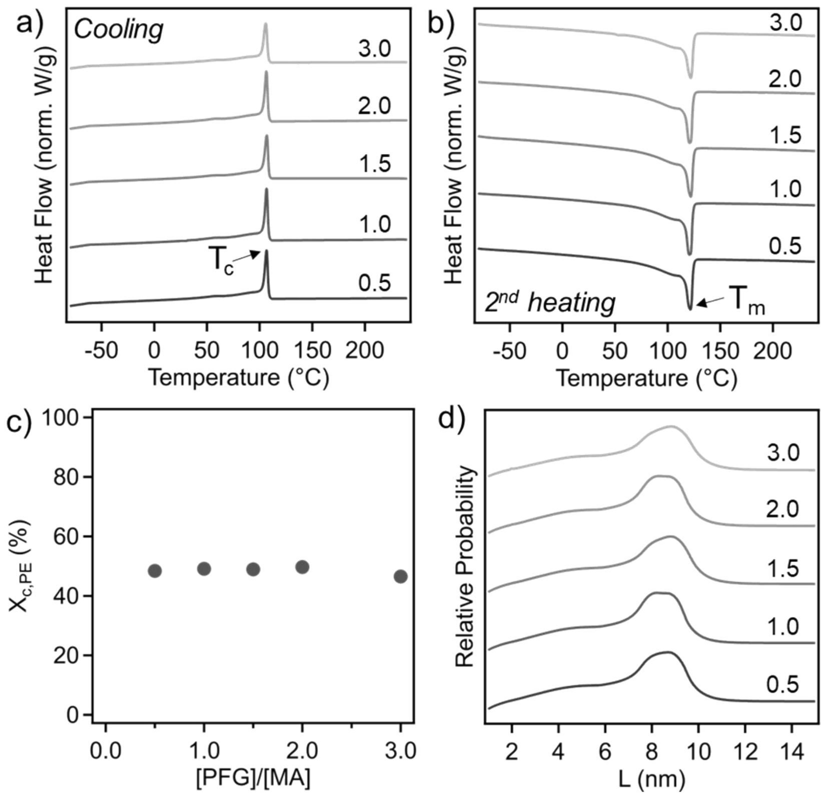

Figure S12. PE_b DSC a) cooling and b) heating curves showing the T_c and T_m, respectively. c) Degree of crystallization normalized to the PE content. d) Relative probability of lamellar thickness melting and crystallization curves for PE_b materials.

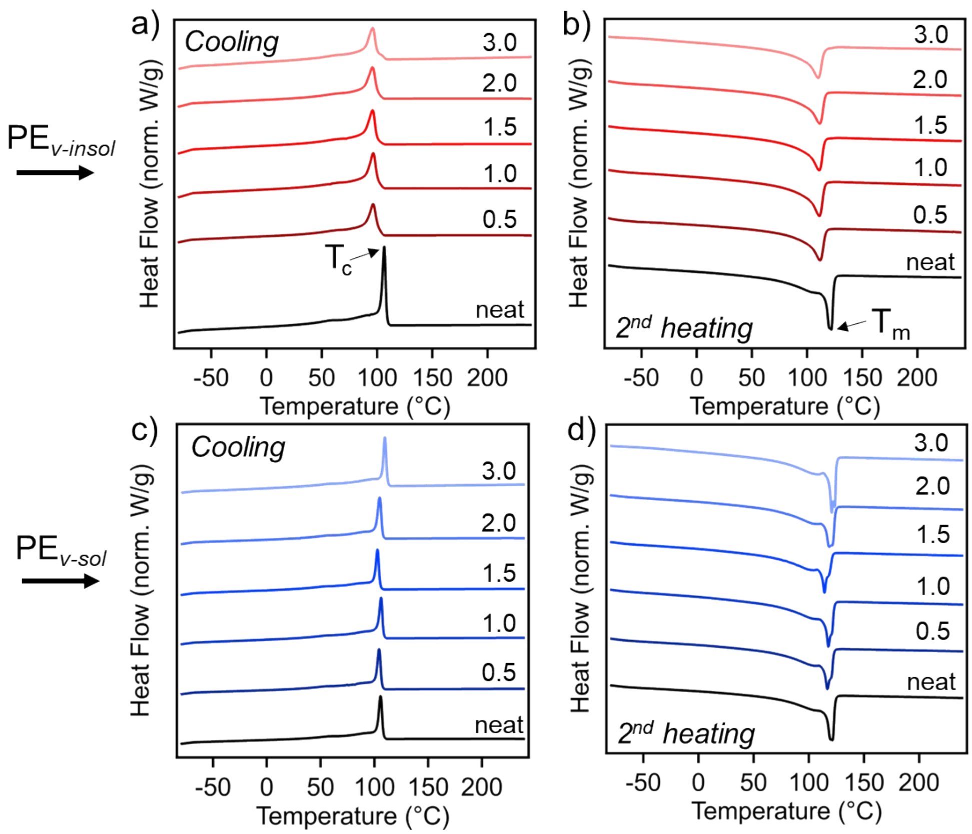

Figure S13. DSC cooling and heating thermograms of a) and b) $PE_{v\text{-}insol}$ versus c) and d) $PE_{v\text{-}sol}$.

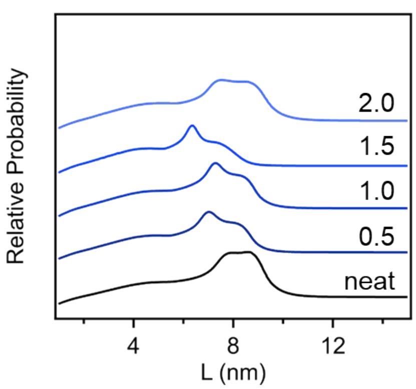

Figure S14. Relative probability of $PE_{v\text{-}sol}$ L populations.

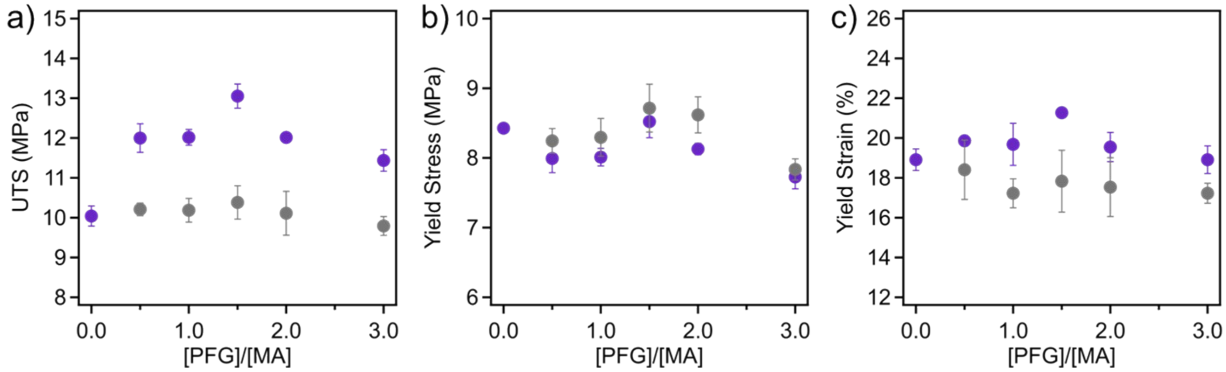

Figure S15. Mechanical properties of PEv (purple) and PEb (gray), specifically, a) UTS, b) yield stress, and c) yield strain.

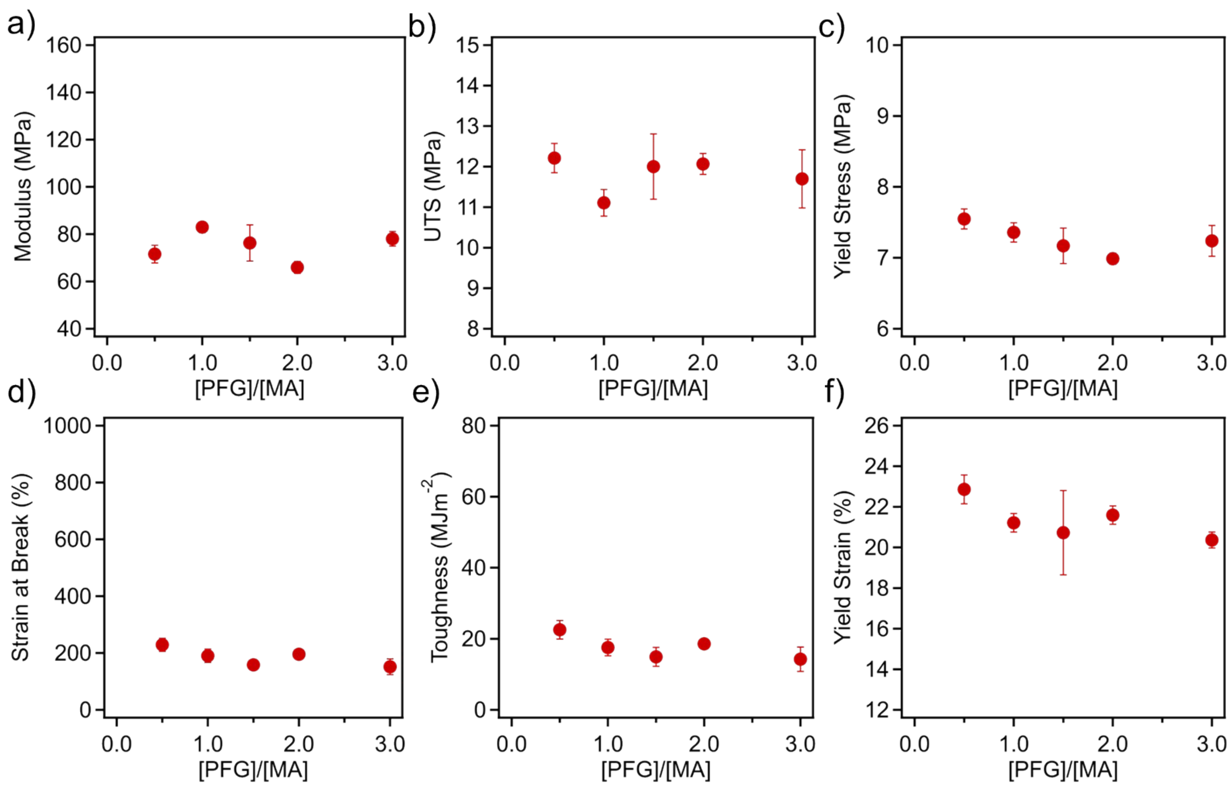

Figure S16. Mechanical properties of $PE_{v\text{-}insol}$ materials as a function of POSS loading, including a) modulus, b) UTS, c) yield Stress, d) strain at break, e) toughness, and f) yield strain.

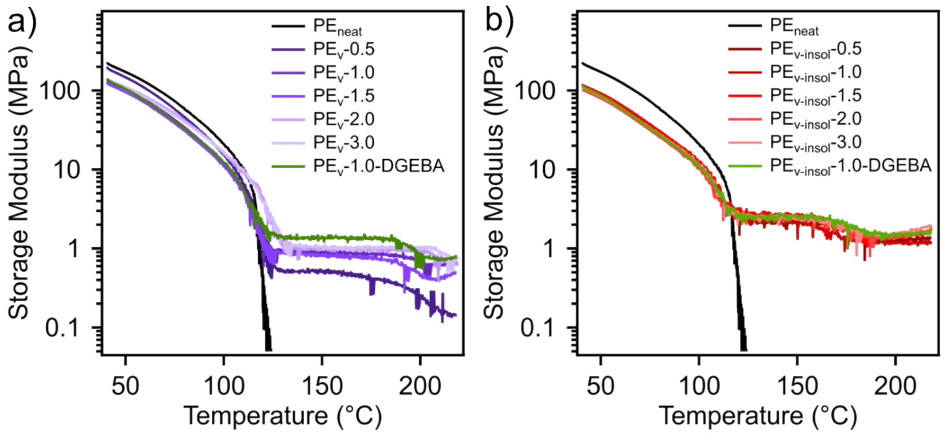

Figure S17. DMA showing the storage modulus over a temperature ramp for (a) PE_v-1.0-DGEBA (green) alongside PE_{neat} (black) and PEv samples (purple), and (b) $PE_{v\text{-}insol}$-1.0-DGEBA (green) alongside PE_{neat} (black) and $PE_{v\text{-}insol}$ samples (red).

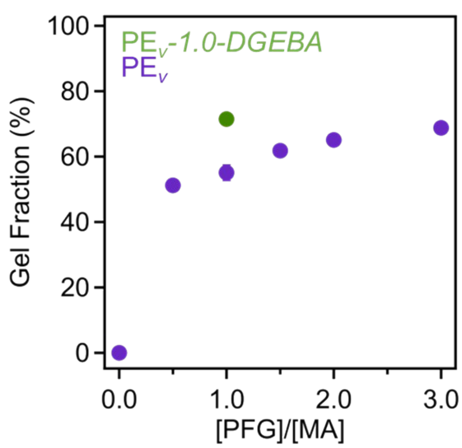

Figure S18. Gel fraction of PE_v-1.0-DGEBA (green) alongside the GPOSS PE_v samples.

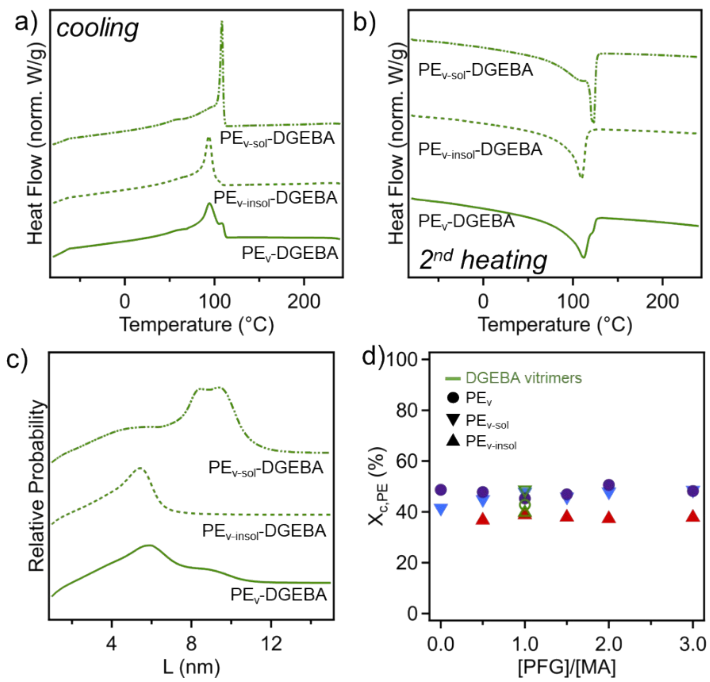

Figure S19. DSC a) cooling and b) second heating thermograms, c) relative probability of lamellar thickness, and d) $\chi_{c,PE}$ for PE$_v$-DGEBA, PE$_{v\text{-}insol}$-DGEBA, and PE$_{v\text{-}sol}$-DGEBA.

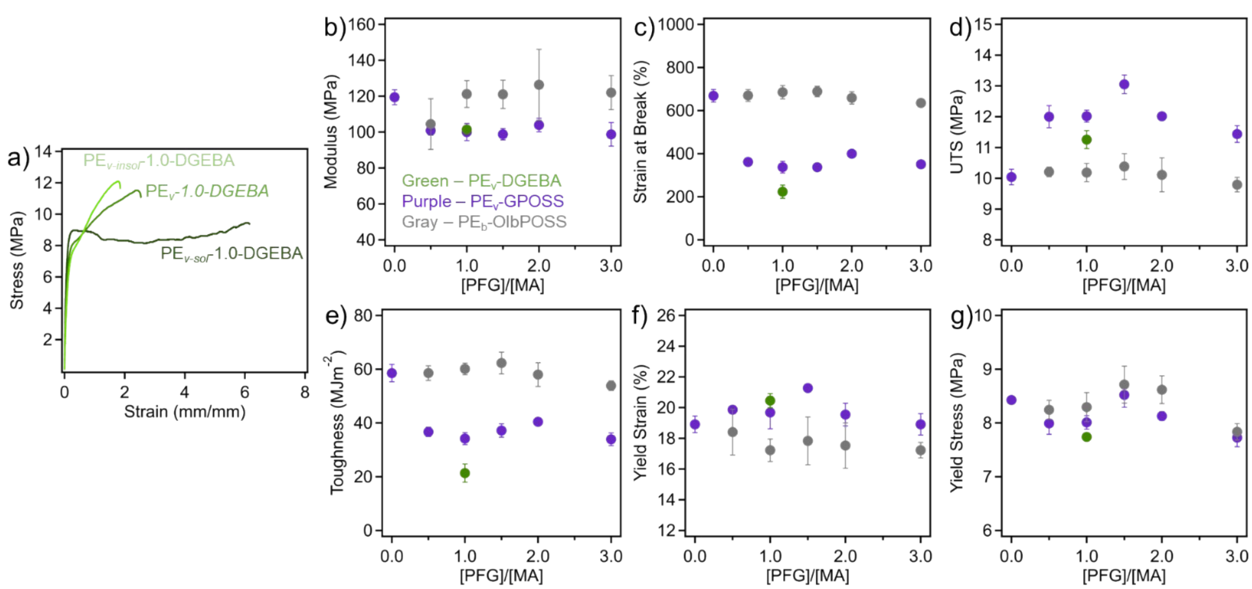

Figure S20. a) Representative stress strain curves for PE$_v$-1.0-DGEBA, PE$_{v\text{-}insol}$-1.0-DGEBA, and PE$_{v\text{-}sol}$-1.0-DGEBA. Extracted mechanical properties of PE$_v$-DGEBA (green) alongside GPOSS PE$_v$ (purple), and OIbPOSS PE$_b$ (gray), including b) modulus, c) strain at break, d) UTS, e) toughness, f) yield strain, and g) yield stress.

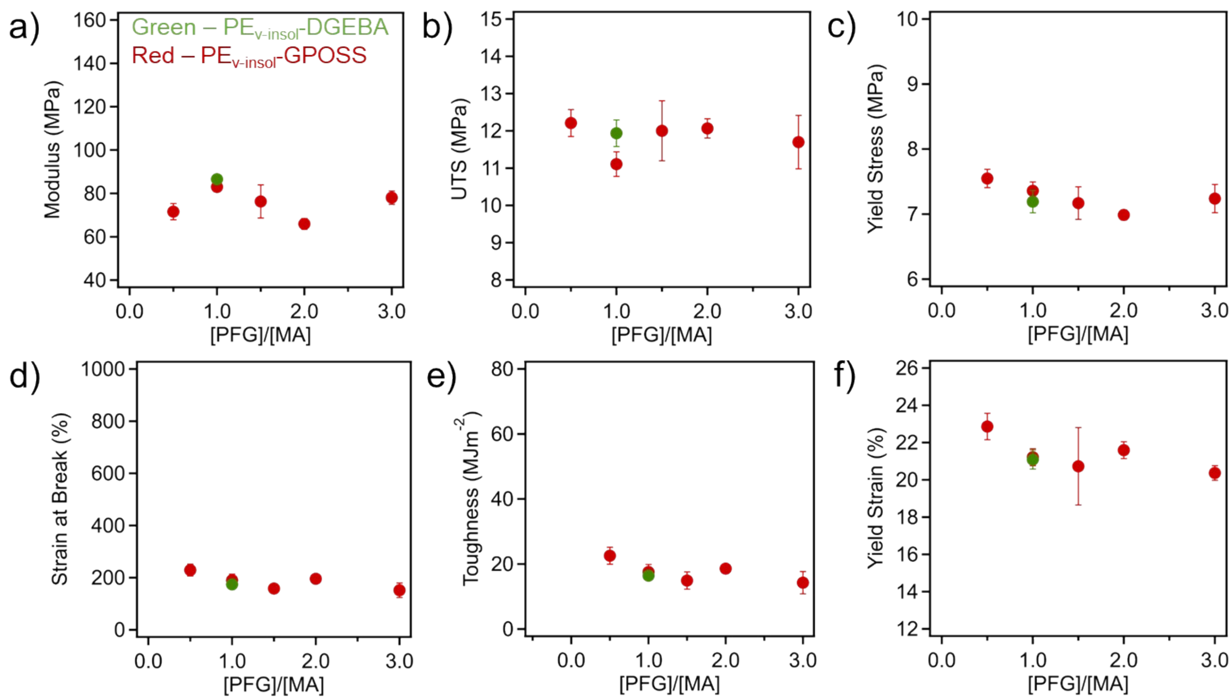

Figure S21. Mechanical properties of $PE_{v\text{-}insol}$-DGEBA (green) alongside mechanical properties of GPOSS-crosslinked $PE_{v\text{-}insol}$ materials (red), including a) modulus, b) UTS, c) yield stress, d) strain at break, e) toughness, and f) yield strain.

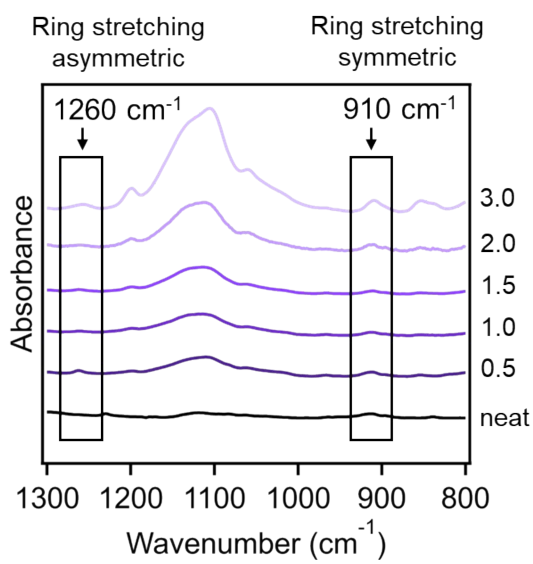

Figure S22. FTIR spectra of the PE_v samples showing epoxide-related stretching bands, specifically 1260 cm^{-1} indicating asymmetric ring stretching, and 910 cm^{-1} indicating symmetric ring stretching.